AGU PUBLICATIONS

JGR

Journal of Geophysical Research: Atmospheres

RESEARCH ARTICLE
10.1002/2016JD025549

Persistent landfalling atmospheric rivers over the west coast of North America

Ashley E. Payne[1] and Gudrun Magnusdottir[1]

[1]Department of Earth System Science, University of California, Irvine, California, USA

Key Points:
- Landfalling AR duration along the western U.S. coastline is quantified
- Spatially and temporally persistent ARs have distinct dynamical and thermodynamical characteristics from AR climatology
- Moisture content rather than dry dynamics appear to be the main contributor to AR persistence

Correspondence to:
A. E. Payne,
aepayne@umich.edu

Citation:
Payne, A. E., and G. Magnusdottir (2016), Persistent landfalling atmospheric rivers over the west coast of North America, *J. Geophys. Res. Atmos.*, *121*, 13,287–13,300, doi:10.1002/2016JD025549.

Received 20 JUN 2016
Accepted 6 NOV 2016
Accepted article online 11 NOV 2016
Published online 22 NOV 2016

Abstract Landfalling atmospheric rivers (ARs) are linked to heavy precipitation and extreme flooding, and are well known along the western coast of North America. The hydrological impacts of ARs upon landfall are correlated with their duration and magnitude. In order to improve the forecast of these hydrologically significant landfalling events, a better understanding of how they differ from other landfalling events must be established through an investigation of the mechanisms leading to their development prior to landfall. A subset of persistent landfalling AR events between 30°N and 50°N is identified in 3-hourly Modern-Era Retrospective Analysis for Research and Applications reanalysis and validated against existing data sets. These events are identified as features in the low troposphere with high moisture transport and extended geometry that persist over a limited region of the coastline for longer than 63 h (85th percentile of AR duration). A composite analysis shows that persistent events have distinct thermodynamical and dynamical characteristics compared to all AR events. They are characterized by greater moisture content, suggestive of Pineapple Express-type events, a perturbed upper level jet and anticyclonic overturning of potential vorticity contours associated with anticyclonic Rossby wave breaking. Moreover, the location of the Rossby wave breaking is shifted inland compared to all AR events. Analogue analysis of the 500 hPa geopotential height anomalies is used to find nonpersistent events with similar dynamical characteristics to persistent events. Despite their similarity to persistent events, nonpersistent analogues show very little shift toward longer duration. A comparison of the development of persistent and nonpersistent analogues shows that persistent events have much greater moisture content.

1. Introduction

Atmospheric rivers (ARs) are synoptic-scale, filamentary features with high water vapor content in the lower troposphere that have been shown to play an important role in the regional hydrology of the western coastline of North America. Their interaction with topography and inland extension are linked to heavy precipitation and flooding [*Ralph et al.*, 2005, 2006; *Dettinger*, 2011; *Ralph and Dettinger*, 2012; *Rivera et al.*, 2014]. However, despite their extreme nature, ARs have also been shown to be an important source of water to the region on climatological scales, contributing up to 50% of total water resources [*Guan et al.*, 2010; *Dettinger*, 2011]. Therefore, a greater understanding of the processes leading up to the most persistent and, locally, the most precipitation producing ARs is essential to the region.

ARs exhibit a wide range of characteristics at landfall. Variability in these characteristics contributes to the large interannual variability in total precipitation found over the region [*Dettinger et al.*, 2011; *Ralph and Dettinger*, 2012]. Along the western coastline of North America, in particular, the characteristics of landfalling events are well described in recent literature [e.g., *Neiman et al.*, 2008b; *Warner et al.*, 2012; *Rutz et al.*, 2014]. Along with precursor soil moisture conditions, the duration and the magnitude of vertically integrated moisture transport of landfalling AR events are strongly associated with their hydrological impacts [*Ralph et al.*, 2013; *Moore et al.*, 2012]. The effects of a nearly stationary AR on precipitation amounts was documented in *Moore et al.* [2012] in a case study of a single AR that contributed heavy rainfall and flooding in a different region over a 2 day period in May 2010. In a more detailed investigation, *Ralph et al.* [2013] documented the hydrological characteristics of landfalling events over a 6 year period using station-based observations near the Russian River basin in California. While the average duration of events passing over this region was 20 h, persistent events in excess of 40 h were observed. Little work has been done to investigate the large-scale patterns contributing to the development of *persistent* ARs along the western coastline of North America. While previous work has focused on the characteristics of cold-season flood events over the region

[e.g., *Lackmann and Gyakum*, 1999], we focus only on the characteristics of ARs, which describe a large subset of such episodes [*Dettinger*, 2013]. Such an investigation is essential in order to improve forecast skill of these hydrologically significant landfalling events.

Our aim is to investigate the large-scale characteristics of persistent AR events over the North American west coast. Here we address the question of how these events are different from "normal" AR events. Our data and methods are described in section 2. A description of the data set of landfalling events used in this investigation and a composite analysis of persistent AR events are shown in sections 3.1 and 3.2. An application of circulation analogue analysis and discussion of the association of subtropical moisture with persistent events are shown in section 3.3. Conclusions are found in section 4.

2. Data and Methods

2.1. Data

We use the Modern-Era Retrospective Analysis for Research and Applications (MERRA) reanalysis data set, available from 1979 [*Rienecker et al.*, 2011]. This data set has been used in previous studies on ARs [e.g., *Lavers et al.*, 2012; *Ryoo et al.*, 2013; *Payne and Magnusdottir*, 2014], and its performance in the identification of AR features has been evaluated against satellite data [*Jackson et al.*, 2016]. Geopotential height (Z), sea level pressure (SLP), and potential vorticity (PV) are retrieved from pressure levels at reduced spatial resolution ($1.25° \times 1.25°$) at 3-hourly intervals. PV on the 350 K isentropic surface is calculated using log linear interpolation of isobaric PV onto potential temperature surfaces. The magnitude of vertically integrated moisture flux (MF) and precipitable water (PW) are calculated as in *Payne and Magnusdottir* [2015]:

$$\mathrm{MF}(\lambda, \phi, t) = g^{-1} \int_{p_s}^{p_t} q(\lambda, \phi, p, t)\, |\mathbf{V}(\lambda, \phi, p, t)|\, \mathrm{d}p \tag{1}$$

and

$$\mathrm{PW}(\lambda, \phi, t) = \left(g \rho_w\right)^{-1} \int_{p_s}^{p_t} q(\lambda, \phi, p, t) \mathrm{d}p, \tag{2}$$

where $|\mathbf{V}|$ is the horizontal wind speed on isobaric surfaces measured in units of m s^{-1}, q is specific humidity measured in units of kg kg^{-1}, g is the gravitational acceleration (9.81 m s^{-2}), ρ_w is the density of water (1000 kg m^{-3}), p_s is 1000 hPa, and p_t is 500 hPa.

Total precipitation and turbulent heat flux (calculated as the sum of net sensible and latent heat fluxes, both of which are positive upward) are retrieved at native spatial resolution ($2/3° \times 1/2°$) at 1-hourly intervals. Precipitation data are converted from units of kg m^{-2} s to units of mm h^{-1}, and the cumulative 3 h precipitation total is calculated (units of mm 3-h^{-1}). Data are linearly interpolated to reduced spatial resolution for use with moisture and dynamical fields.

2.2. Identification of AR Conditions and Event Clustering

While recent works [e.g., *Guan and Waliser*, 2015; *Mundhenk et al.*, 2016] have highlighted the year-round presence of ARs over the North Pacific, our focus is limited to landfalling events and their resulting hydrological impacts along the densely populated North American coastline between 30°N and 50°N. This transect is limited to the western coastline of the contiguous United States and southern Canada to avoid blending the differing seasonal cycles of north and south coast ARs [*Mundhenk et al.*, 2016]. Impacts to this limited region have been shown to occur predominately in the late fall to winter [*Neiman et al.*, 2008b; *Ralph and Dettinger*, 2012; *Mundhenk et al.*, 2016]. Therefore, as in *Payne and Magnusdottir* [2014, 2015], we focus on the winter half year of landfalling ARs defined by their physical proximity to the coastline. Conditions along a transect following the coastline are recorded using 36 seasons of MERRA reanalysis (30°N to 50°N, October–March 1979–2014). We use the following set of criteria based on previous studies to identify AR conditions at each 3-hourly time step: (1) MF $\geq$ 85th percentile (with latitudinal dependence as in *Lavers et al.* [2012]), (2) PW $\geq$ 2 cm [*Ralph et al.*, 2004, 2005; *Neiman et al.*, 2008b], and (3) 850 hPa wind speed $\geq$ 10 m s^{-1} (an approximation from *Ralph et al.* [2004, 2005]). The transect used to record conditions is shown in the inset of Figure 1a and differs slightly from the method in *Payne and Magnusdottir* [2014] as we only consider a single grid point for each latitude for the region hugging the coastline. Since the purpose of this research is to look at the duration of each landfalling event rather than general characteristics, averaging over a zonal section as in

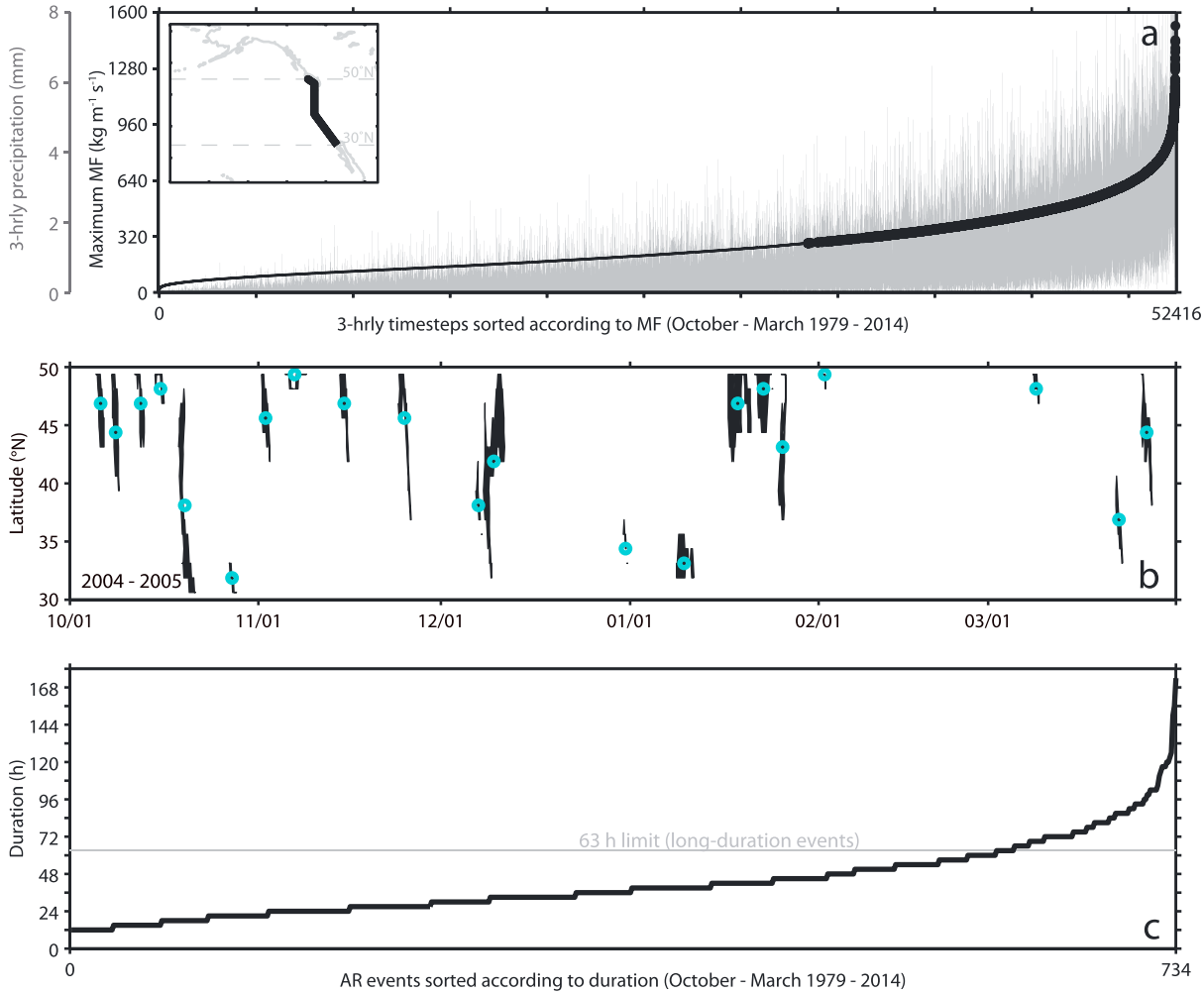

Figure 1. Using MERRA reanalysis, (a) all 3-hourly time steps in the winter season (October–March 1979–2014) sorted according to the maximum magnitude of integrated moisture transport (MF, black line) as detected along the transect. Associated precipitation totals for each time step are shown in grey. Identified AR conditions are shown as filled black circles. (b) As an example, identified AR events for the 2004–2005 winter season, with the median landfalling latitude marked as a teal open circle. (c) All identified AR *events* sorted according to duration, with long-duration events falling above the 63 h limit (persistent events as described in the text have an additional limitation of less than 6° latitudinal variance).

Payne and Magnusdottir [2014] may introduce uncertainty in the duration of the event by smoothing out its initiation or termination. Figure 1a shows the distribution of all time steps considered, sorted according to peak MF (black line) with associated cumulative 3-hourly precipitation (grey line).

Time steps that are identified as having AR conditions (filled black circles in Figure 1a) are clustered in time into distinct landfalling events by grouping temporally and spatially consistent MF and PW. As our latitudinally dependent thresholds on MF are larger than the generally accepted lower limit of 250 kg m^{-1} s^{-1} [e.g., *Rutz et al.*, 2014], solely for the purposes of feature identification, we use a static threshold of 280 kg m^{-1} s^{-1} (the minimum from the criterion that MF $\geq$ 85th percentile). In order to ensure that the feature fits the definition of an AR while still considering its initiation and termination along the coastline, we require that at least one time step matches the AR criteria described in the previous paragraph and that it exceed 1200 km in length (revised from the 2000 km length when using remotely sensed PW [e.g., *Rutz et al.*, 2014]) at least once in its lifetime. To reduce false identification, AR conditions must persist along the coastline for longer than 12 h [e.g., *Ramos et al.*, 2015] and the latitude at which the feature intersects the coastline must be consistent with adjacent time steps. For example, a series of time steps in which peak MF is recorded at 36°N, 52°N, 55°N, and 33°N would not describe a cohesive event. Compare that example to a series of time steps in which peak MF is recorded at 36°N, 35°N, 34°N, and 33°N, which would describe a cohesive event. The overall variance of each event is composed of all latitudes recorded over its lifespan. After automated identification, events are

visually verified as coherent structures. As an example, Figure 1b shows the latitudinal position (y axis) and date (x axis) of identified landfalling events for the 2004–2005 winter season. The average latitudinal position of each event is shown as an unfilled teal circle. Figure 1c shows all AR events identified (734 total), sorted by duration (in hours). We identify *persistent events* as those that persist over the coastline for more than 63 h (determined from the 85th percentile of duration) and have a latitudinal variance of less than 6° latitude. This results in a total of 66 persistent ARs.

2.3. Rossby Wave Breaking Detection

In an earlier study [*Payne and Magnusdottir*, 2014] we found that almost all wintertime landfalling North Pacific (between 20°N and 60°N) ARs are associated with anticyclonic Rossby wave breaking (RWB). RWB is defined as the rapid and irreversible overturning of PV contours on isentropic surfaces [*McIntyre and Palmer*, 1983]. For the purposes of investigating the large-scale characteristics of landfalling events, we examine the role of RWB. Figure 2a, depicting PV contours on the 350 K surface on 0000 UTC 9 Oct 1979, shows an example of anticyclonic RWB associated with a persistent landfalling AR. The location and zonal extent of each breaking event is quantified using a RWB detection algorithm from *Strong and Magnusdottir* [2008b] and adapted to 3-hourly 350 K PV data from MERRA (coarsened to a resolution of 2.5° × 2.5° using linear interpolation). At each PVU (1 potential vorticity unit (PVU) $\equiv 10^{-6}$ m^2 s^{-1} K kg^{-1}) between 0 and 20, the longest circumpolar PV contour is identified. When overturning is detected (contour crosses a meridian more than once), we record the location of the centroid of the breaking "bay" and its zonal extent (L, calculated as the degree arc length of a great circle passing through the centroid and spanning the breaking bay), and the *PV* contour on which the breaking is detected (for details, see appendix in *Strong and Magnusdottir* [2008b]). For each bin centered on (λ, ϕ) and numbered $n = 1, \ldots, N$, the relative frequency of breaking (γ) is calculated as follows:

$$\gamma(\lambda,\phi)_n \equiv \frac{1}{T}\sum_{t=1}^{T}\beta\left[(\lambda,\phi)_n, t\right] \tag{3}$$

where

$$\beta\left[(\lambda,\phi)_n, t\right] = \begin{cases} 1 & \text{if centroid is present} \\ 0 & \text{otherwise} \end{cases} \tag{4}$$

and where T is the total number of 3-hourly observations.

2.4. Statistical Methods

2.4.1. Significance

Composite analysis is used to compare persistent AR events to all AR events. A block bootstrap technique is used to assess the statistical significance of the differences between persistent ARs and all ARs in order to account for autocorrelation within the data set. Over 1000 iterations, composites are calculated using events (composed of multiple 3-hourly time steps) that are randomly sampled with replacement from the data set of all AR events. At each grid point, the value in each subset is determined to be statistically significant at the 95% level if it exceeds the confidence interval from the bootstrap sample composites. In composite maps, significance is indicated by grey stippling.

2.4.2. Analogue Analysis

We investigate the role of the large-scale atmospheric circulation in the modulation of AR persistence using circulation analogue analysis [*Lorenz*, 1969]. By this method, we test the hypothesis that if dry dynamics play an important role in AR duration, nonpersistent events with analogous circulation anomalies will have longer durations than the average of all AR events. We note that this is a simple approach and more robust results require the use of perturbation experiments. Our focus is on extreme episodic wintertime events; therefore, we do not limit our data set by the seasonality of circulation changes as in, for example, *Lorenz* [1969] and *Vautard and Yiou* [2009], and consider all nonpersistent events, with nonoverlapping time steps, as possible analogues to persistent events. It should be noted that persistent events have the added criterion on location of landfall, so it is possible for events with relatively longer durations to be selected as nonpersistent analogues.

We use 500 hPa geopotential height anomalies (over the region 20°N–60°N, 180°W–80°W) to quantify the large-scale characteristics of each AR event. Anomalies are calculated from the daily climatology at each grid point. For each persistent event, we find the median of the closest five nonpersistent analogues from the data set of all nonpersistent AR events. Potential analogues are not allowed to fall within 15 days of the event to

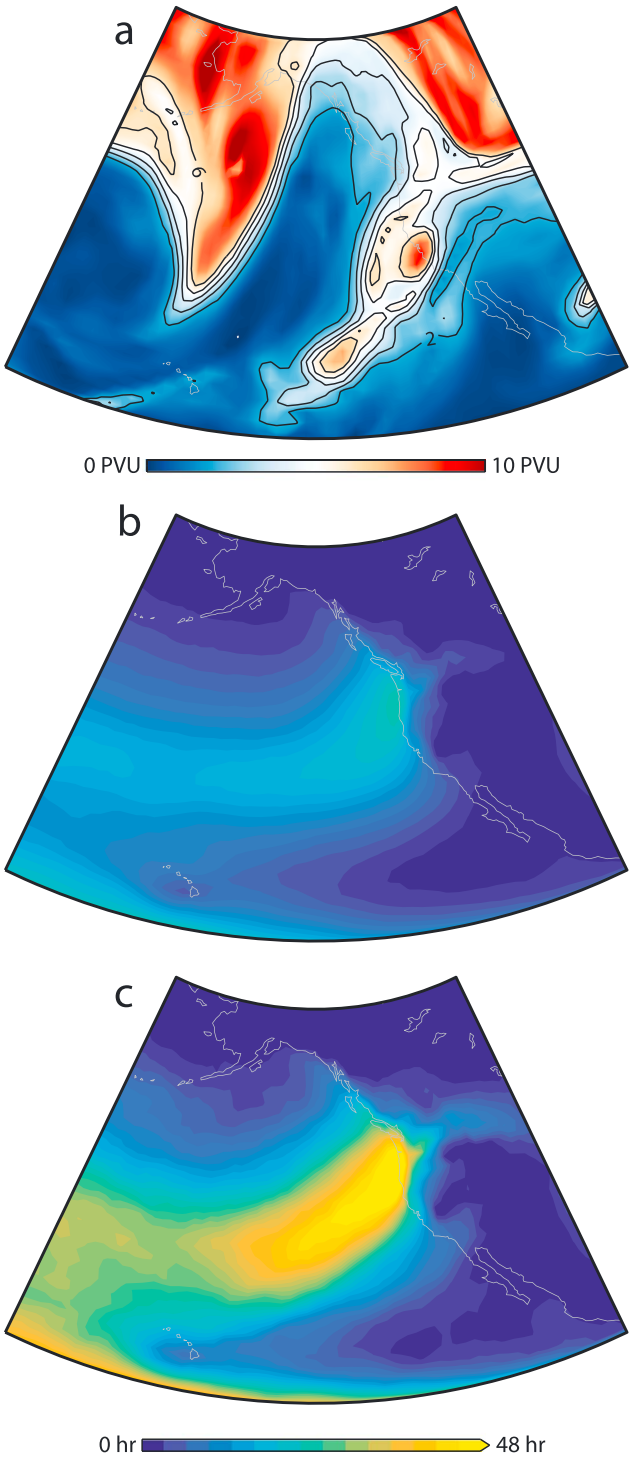

Figure 2. (a) An example of the 350 K PV field for a persistent event occurring on 0000 UTC 9 October 1979. Contours begin at 2 PVU and increase in increments of 1 PVU to 6 PVU. The average duration of (b) all ARs and (c) persistent ARs. Duration is calculated as the average number of time steps with MF $\geq$ 250 kg m^{-1} s^{-1}.

avoid overlap. Similarity is objectively determined using the Pearson rank correlation coefficient [e.g., *Vautard and Yiou*, 2009]. Correlations are quite high and range from 0.54 to 0.93, with the majority falling above 0.74. The composite development of this subset of nonpersistent AR events with the highest correlation coefficients is compared to that of persistent events at 48 and 24 h prior to landfall.

3. Results

We break our results into three parts. First, we discuss the characteristics of our persistent landfalling AR data set and compare it to existing records of AR landfall. Second, we examine how the persistent ARs are different from all landfalling ARs. We finish with a comparison of the development of nonpersistent analogues to persistent events by applying circulation analogue analysis.

3.1. Overview of the Data Set of Persistent ARs

Many AR identification schemes exist in the literature [e.g., *Lavers et al.*, 2012; *Guan and Waliser*, 2015]; however, few can be applied to an analysis of AR duration. Outside of case studies, identification schemes generally identify time steps with AR conditions rather than multi–time step events. To place our results in context, we compare our data set of landfalling AR events against existing records. The global reanalysis-based data set developed in *Guan and Waliser* [2015] was examined over the west coast region and has 90% overlap with our AR event data set. Our data set is in good agreement with older records that use satellite-derived humidity observations (no wind) to identify landfalling events in total column precipitable water [*Neiman et al.*, 2008b], with 80% overlap. Given the differences in the data sets used, the addition of a 2 day buffer increases agreement to 97% with *Guan and Waliser* [2015] and to 88% with *Neiman et al.* [2008b]. All notable landfalling events singled out in the literature are captured by our data set [e.g., *Leung and Qian*, 2009; *Galewsky and Sobel*, 2005; *Ralph et al.*, 2003, 2006, 2011; *Smith et al.*, 2010; *Neiman et al.*, 2008a, 2011]. We note that the purpose of developing the data set used in this research is not to present an alternative to already available AR identification methods but rather to supplement these records with added information on persistence that, to the best of our knowledge, is not yet available.

Over the 36 seasons considered in this investigation, 7119 3-hourly time steps are identified as having landfalling conditions (MF $\geq$ 85th percentile, PW $\geq$ 2 cm, 850 hPa wind speed $\geq$ 10 m s^{-1}). These time steps are clustered into 734 landfalling events, for an average of 20 events per season, with lifetimes along the coastline ranging from 12 to more than 150 h. Sixty-six events are identified as persistent (duration along the coastline exceeds the 85th percentile (63 h) and latitudinal variance is less than 6°). Consistent with a similar analysis in *Ramos et al.* [2015] and with findings in *Ralph et al.* [2013], the majority of the identified AR events last between 12 and 48 h and only a fraction persist for longer than 63 h (Figure 1c). The seasonal distribution of persistent events does not show any significant departures from that of all AR events. Most persistent events occur early in the season (October–December) with fewer later in the season (January–March).

To visualize the differences between the two data sets (persistent versus all AR events), we compare the average duration of AR conditions (calculated as MF $\geq$ 250 kg m^{-1} s^{-1}) in Figures 2b and 2c, following the technique used in *Rutz et al.* [2014]. Each panel shows a composite over all events of the average number of time steps during which AR conditions are satisfied at each grid point. Consistent with work in *Rutz et al.* [2014], regions with the highest AR frequency of occurrence are colocated with regions with the highest duration (not shown). Both data sets show inland penetration in the Pacific Northwest and, to a lesser degree, along the coastline of Southern California. Average duration peaks along the coastlines of Washington and Oregon with a maximum of 36 h in Figure 2b and a maximum of 72 h in Figure 2c. The agreement of this data set with established records and the clear difference in average duration between persistent and all AR events supports its use for an investigation of variability in the timing of landfalling events.

3.2. Differences in Persistent ARs Compared to All ARs

The purpose of this section is to determine what differences exist at the large-scale between persistent events and all AR events. To do this, we show in Figures 3 and 4 the composite difference between the two groups, starting with moisture fields in Figure 3 and extending our analysis to dynamical fields in Figure 4. In each panel, the field for all ARs is shown in contours, the difference field (persistent ARs − all ARs) is shown in shading and significance at the 95% level is indicated by grey stippling.

Positive precipitation anomalies during persistent events are concentrated along the coastline of the Pacific Northwest (Figure 3a), in agreement with the region of maximum average duration shown in Figure 2c.

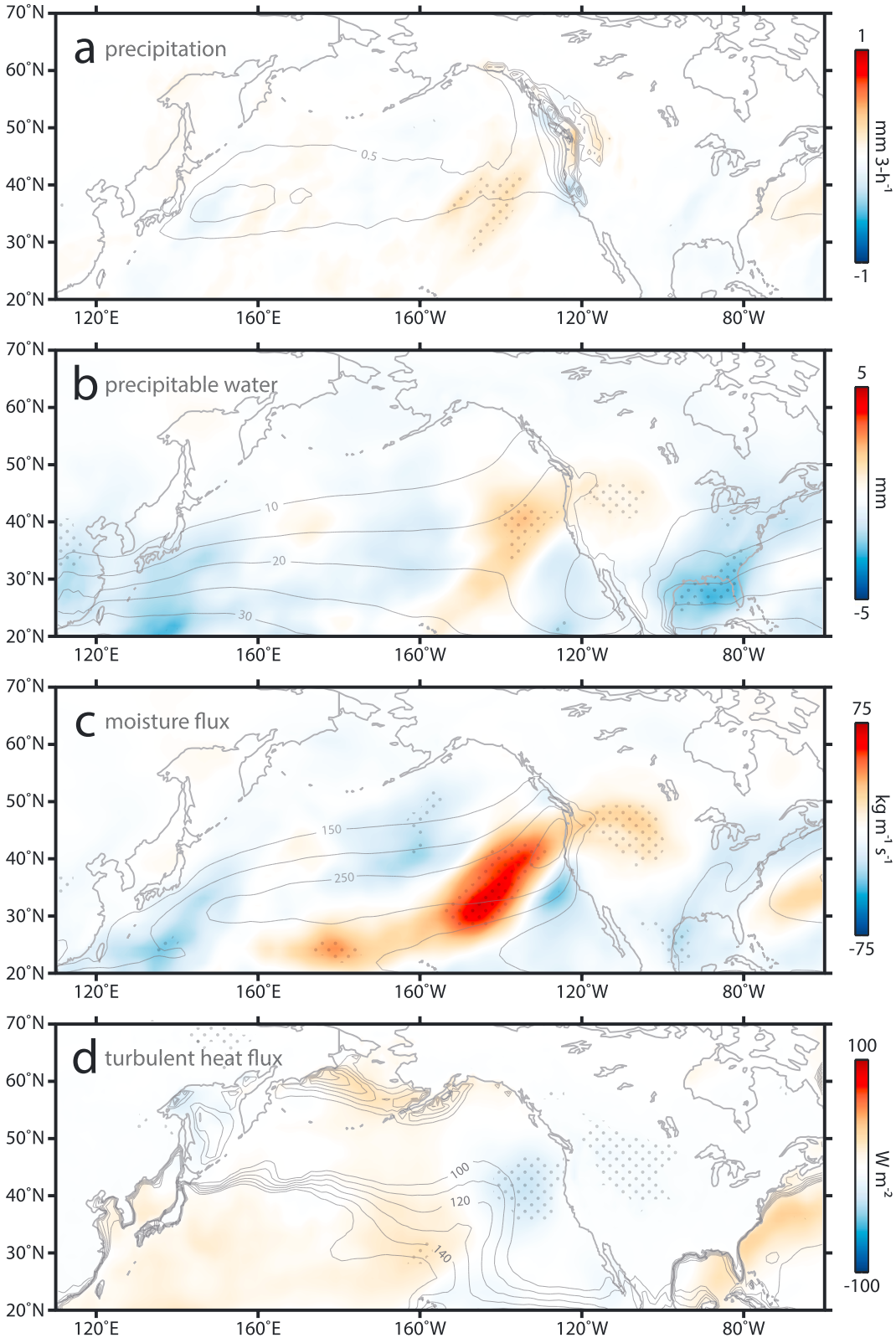

Figure 3. For all panels, the composite of all AR events is shown in contours. Persistent AR events minus the all AR climatology is shown in shading. Grey stippling shows statistical significance at the 95% level. (a) For total precipitation ((mm 3-h^{-1}, contours in intervals of 0.25 mm 3-h^{-1}, starting from 0.5 mm 3-h^{-1}).), (b) PW (mm, contours in intervals of 5 mm, starting from 10 mm), (c) MF (kg m^{-1} s^{-1}, contours in intervals of 50 kg m^{-1} s^{-1}, starting from 150 kg m^{-1} s^{-1}), and (d) turbulent heat flux (W m^{-2}, contours in intervals of 10 W m^{-2}, starting from 100 W m^{-2}).

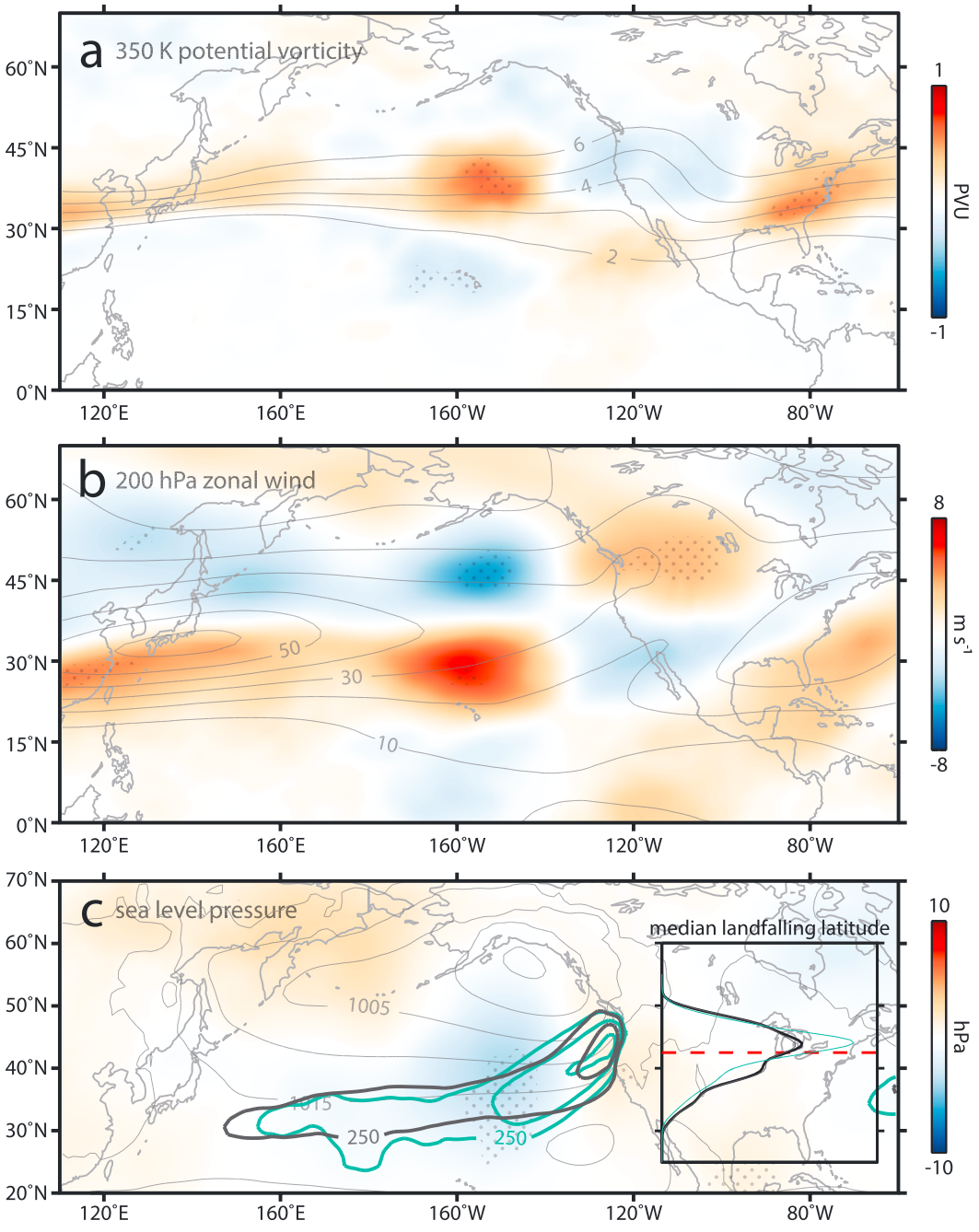

Figure 4. Same as Figure 3 but for (a) 350 K PV (PVU, contours in intervals of 1 PVU, starting from 2 PVU), (b) 200 hPa zonal wind (m s^{-1}, contours in intervals of 10 m s^{-1}, with the zero contour omitted), and (c) SLP (hPa, grey contours in intervals 7 hPa, starting from 980 hPa). Colored contours in Figure 4c show composite MF for persistent (teal) ARs and all ARs (grey) (intervals of 100 kg m^{-1} s^{-1}, starting from 250 kg m^{-1} s^{-1}). The inset in Figure 4c shows a probability density function (pdf) of the median landfalling latitude for all 734 events with the division at 42.5°N in red. Pdfs of all ARs (excluding persistent events) are shown in grey and of persistent ARs are shown in teal.

Despite well-documented hydrologically significant events impacting the southern part of the domain, such as the New Year's Day event of 1997 [*Leung and Qian*, 2009], negative precipitation anomalies that cover the region suggest that the persistent event subset is dominated by events mainly affecting the northern part of the domain. Regional differences in the characteristics of landfalling events over the North Pacific is a point that has been touched on by previous researchers [i.e., *Neiman et al.*, 2008b] and will be addressed later in this section.

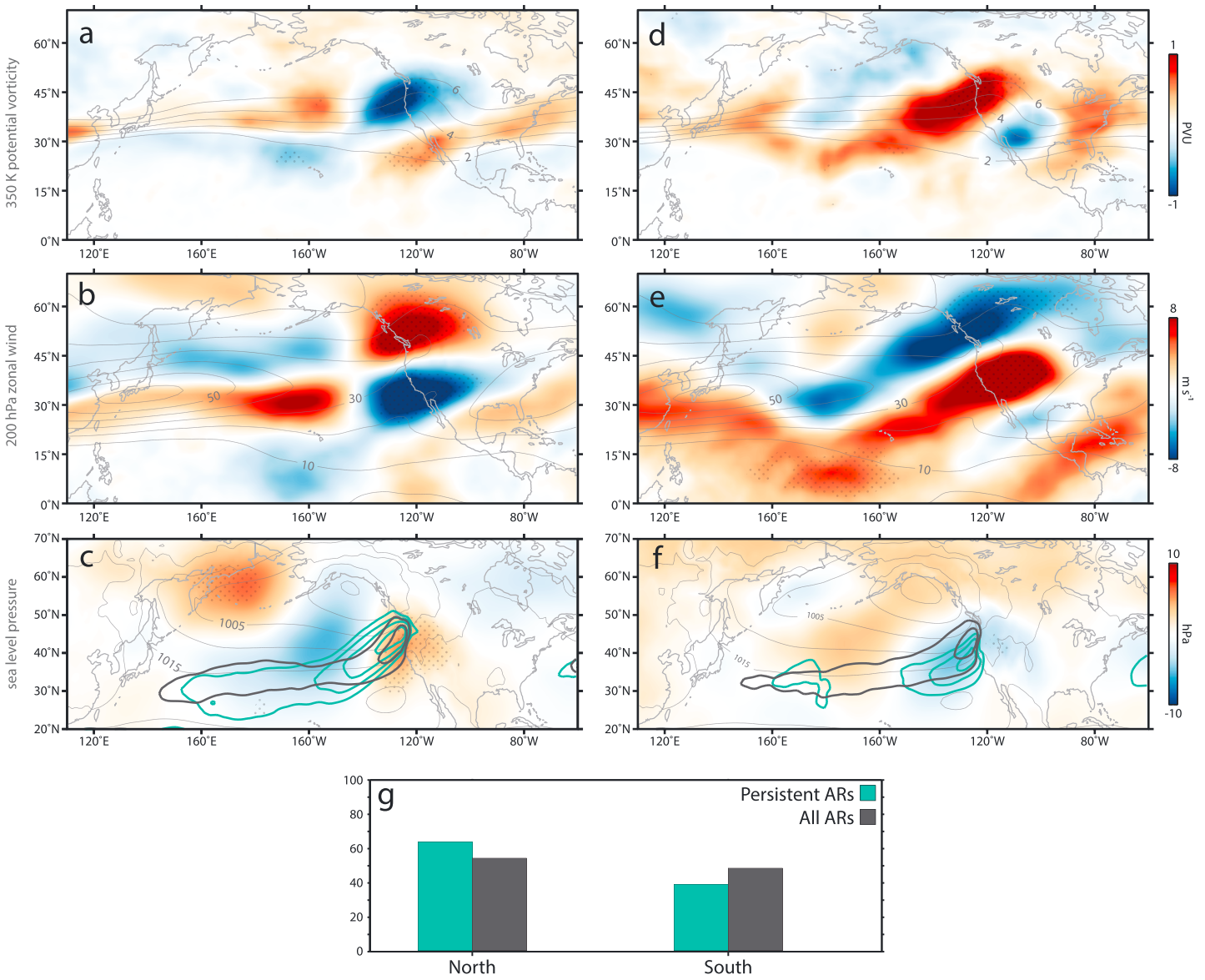

Figure 5. Same as Figure 4 but for (a–c) ARs making landfall north of 42.5°N and (d–f) ARs making landfall south of 42.5°N. (g) Percentage of persistent ARs that make landfall on the north coast are shown in teal (on the left), and the persistent ARs that make landfall on the south coast are shown in teal (on the right). Grey boxes show percentages between north and south for all ARs.

Consistent with the distribution of precipitation anomalies, extensive positive anomalies in PW and MF extend from near Hawaii toward the Pacific Northwest (Figures 3b and 3c, respectively). Negative anomalies in surface turbulent heat flux over the east Pacific (Figure 3d) are consistent with the increased precipitation (Figure 3a), moisture content (Figure 3b), and moisture flux (Figure 3c) in the area of persistent events. The anomalous moisture transport from near Hawaii suggests that persistent events are strongly associated with Pineapple Express events (as described in *Dettinger et al.* [2011]). Pineapple Express events are a subset of landfalling AR events that are characterized by intense moisture transport and warm, heavy precipitation anomalies along the coastline. Our results that were obtained using the three criteria listed earlier thus identify Pineapple Express events as contributing to AR persistence.

In Figure 4, we turn our focus to the large-scale dynamics contributing to the differences between the two data sets. Figure 4a shows the difference in 350 K PV between persistent ARs and all ARs in shading. For a specific example, refer to Figure 2a, which shows an example of the instantaneous overturning PV field associated with one persistent AR event. The persistent landfalling ARs are associated with exaggerated overturning of

PV contours, both larger in amplitude and more equatorward extended than the composite of all ARs. The anticyclonic overturning apparent in the composite is a robust feature that is found for all but one persistent event. This is consistent with other dynamical fields shown in Figures 4b and 4c. The 200 hPa zonal wind anomalies for the persistent ARs (Figure 4b) show a zonally extended jet that is more perturbed downstream in the extratropics, consistent with Figures 2a and 4a. Note that the zonal wind perturbation reaching low latitudes, near 120°W, may be signatures of remainders from previous breaking events (see Figure 2a) or positive PV anomalies characteristic of higher latitudes on the 350 K surface reaching deep into the tropics, also called PV intrusions [*Waugh and Polvani*, 2000]. The east Pacific is a dynamically active region where RWB occurs frequently in winter [*Strong and Magnusdottir*, 2008b, Figure 2a]. It is also a region where anticyclonic RWB has been found to lead to downstream influence over the North Atlantic [e.g., *Strong and Magnusdottir*, 2008a; *Drouard et al.*, 2013].

Figure 4c shows the difference in SLP for the persistent ARs compared to all ARs. The North Pacific low pressure that is typically associated with all ARs [e.g., *Neiman et al.*, 2008b; *Warner et al.*, 2012; *Payne and Magnusdottir*, 2014] is exaggerated for the persistent cases. Persistent events are associated with a broad, deep low-pressure anomaly slightly equatorward of the mean location of the Aleutian Low, consistent with the positive anomalies in PW and MF in Figures 3b and 3c. The ridge of peak moisture transport has a wider areal extent for the persistent cases, indicated by the teal contours in Figure 4c versus the dark grey contours for all ARs.

As mentioned previously, the distribution of moisture anomalies in Figure 3 suggests regional differences in AR behavior. To investigate this, in Figures 5a–5c, we show a regional analysis of Figure 4 for north coast and south coast ARs. Regions are determined from the median of landfalling latitudes over the course of its lifetime along the coastline (shown as a probability density function in Figure 4c). We use the limit of 42.5°N in rough agreement with the domains used in *Neiman et al.* [2008b]. Difference plots show the difference between persistent and all AR events impacting the north coast and south coast, respectively.

North coast only persistent ARs (Figures 5a–5c) are associated with significantly stronger anticyclonic RWB signature over the Pacific Northwest, consistent with a perturbed upper level jet. The North Pacific low-pressure center poleward of the AR is significantly deeper and the negative SLP anomaly in Figure 4c is strengthened. South coast ARs show a very different pattern of anomalies (Figures 5d–5f). The anticyclonic RWB signature seen in Figure 4a is shifted southeastward and is much smaller in extent. The upper level winds show a split jet. These ARs have a broader and weaker low-pressure center to the north with a considerably weaker or nonexistent ridge equatorward of the MF plume. Focusing on the distribution of MF for each region (shown in contour), Figure 5c shows that north coast ARs have the tilted geometry consistent with the positive MF anomalies seen in Figure 3c. This is not the case for the south coast persistent ARs (Figure 5f).

Figure 5g shows the division between north and south coast persistent ARs (teal) and all ARs (grey). The two teal columns add to 100% as do the two grey columns. Figure 5g shows that more of the persistent ARs are located north of 42.5°N. When all ARs are considered (columns in grey), the ARs are divided more equally between the two regions (53% north coast, 47% south coast). When only persistent events are considered, 62% are over the north coast and 38% are over the south coast. The higher frequency of persistent AR events in the northern part of the domain is consistent with general consensus of the climatological behavior of landfalling ARs [e.g., *Neiman et al.*, 2008b].

The frequency of RWB for the background climatological state (October–March 1979–2014) is shown in contours in Figure 6, the difference for persistent ARs compared with all ARs is shown in shading. Consistent with *Payne and Magnusdottir* [2014], most of the RWB events associated with west coast ARs are anticyclonic. In Figure 6a, we show the frequency of anticyclonic RWB. Frequent breaking takes place over the eastern North Pacific with a maximum over the coastline close to 40°N. The shading in Figure 6a shows a significant increase (not shown due to resolution differences) in breaking frequency and a shift in the location of maximum RWB frequency for persistent ARs (persistent ARs minus all ARs) such that the location of maximum wave breaking frequency shifts inland. In Figure 6b we show the same fields except for cyclonic wave breaking. For cyclonic wave breaking, the breaking takes place primarily north of the region of interest. Cyclonic breaking concurrent with persistent ARs is only slightly greater than for all ARs with no spatial shift.

3.3. Development Prior to Landfall

In this section, we compare a subset of nonpersistent analogues to the persistent events described previously. Nonpersistent analogues are selected based on their spatial correlation to each persistent event, so that we are

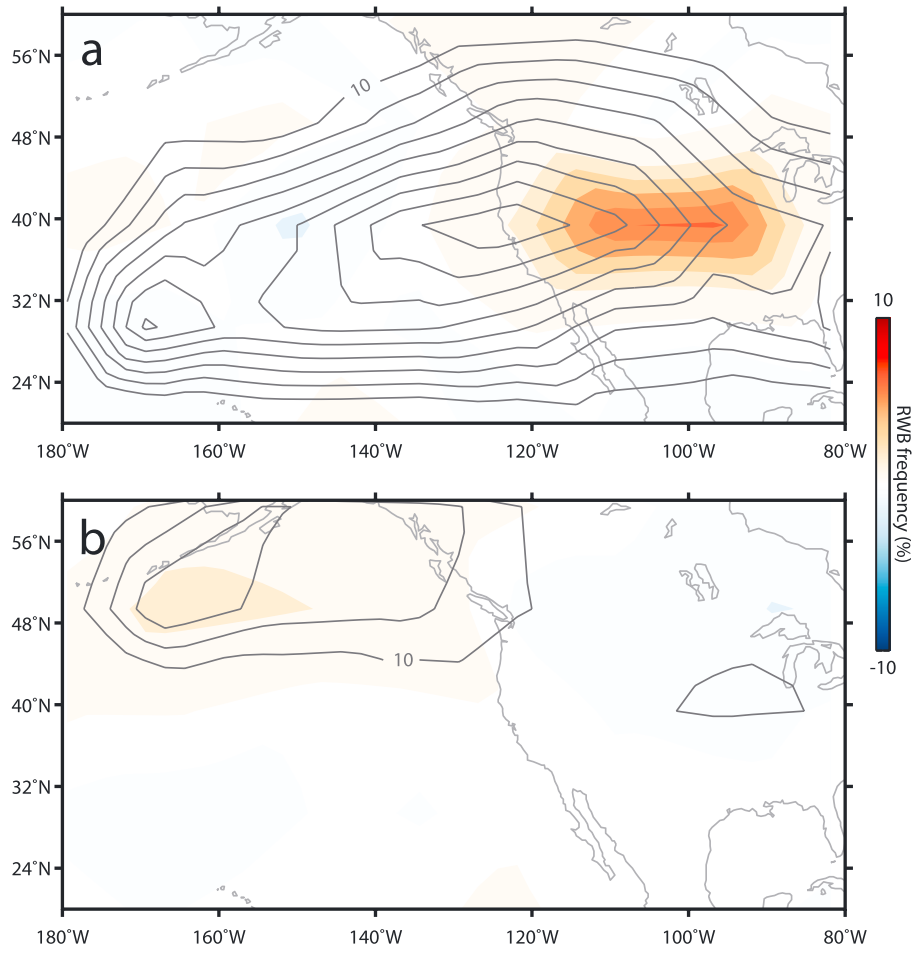

Figure 6. Contours show RWB frequency over October–March 1979–2014 (starting from 10%, increasing in intervals of 1.7%). Shading shows the difference in RWB frequency between persistent and all AR events for (a) anticyclonic and (b) cyclonic breaking events.

left with a data set of 66 nonpersistent analogues. We chose 500 hPa geopotential height anomalies over other fields due to the high degree of separation between events. The motivation for this approach is to determine, in a simple way, whether dry dynamics plays a major role in the persistence of ARs along the coastline. Given similar circulation patterns, if persistence is driven by dry dynamics, nonpersistent analogues should have a considerably higher than average duration compared to all other nonpersistent ARs.

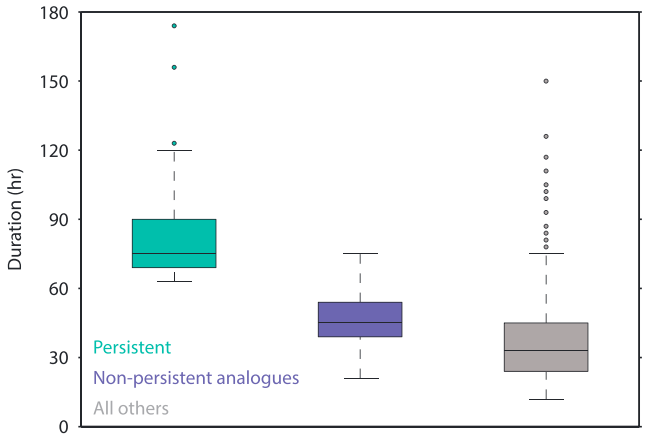

Figure 7. Comparison of AR duration between (teal) persistent ARs, (blue) nonpersistent analogous ARs, and (grey) all other ARs (nonpersistent, nonanalogous).

Indeed, the nonpersistent analogues do have slightly larger median duration than all other nonpersistent, nonanalogue ARs. Figure 7 shows the distribution of duration for persistent ARs, nonpersistent analogues, and all nonpersistent nonanalogue ARs. While the median duration of nonpersistent analogues is slightly higher than that of all other nonpersistent events, the bulk of

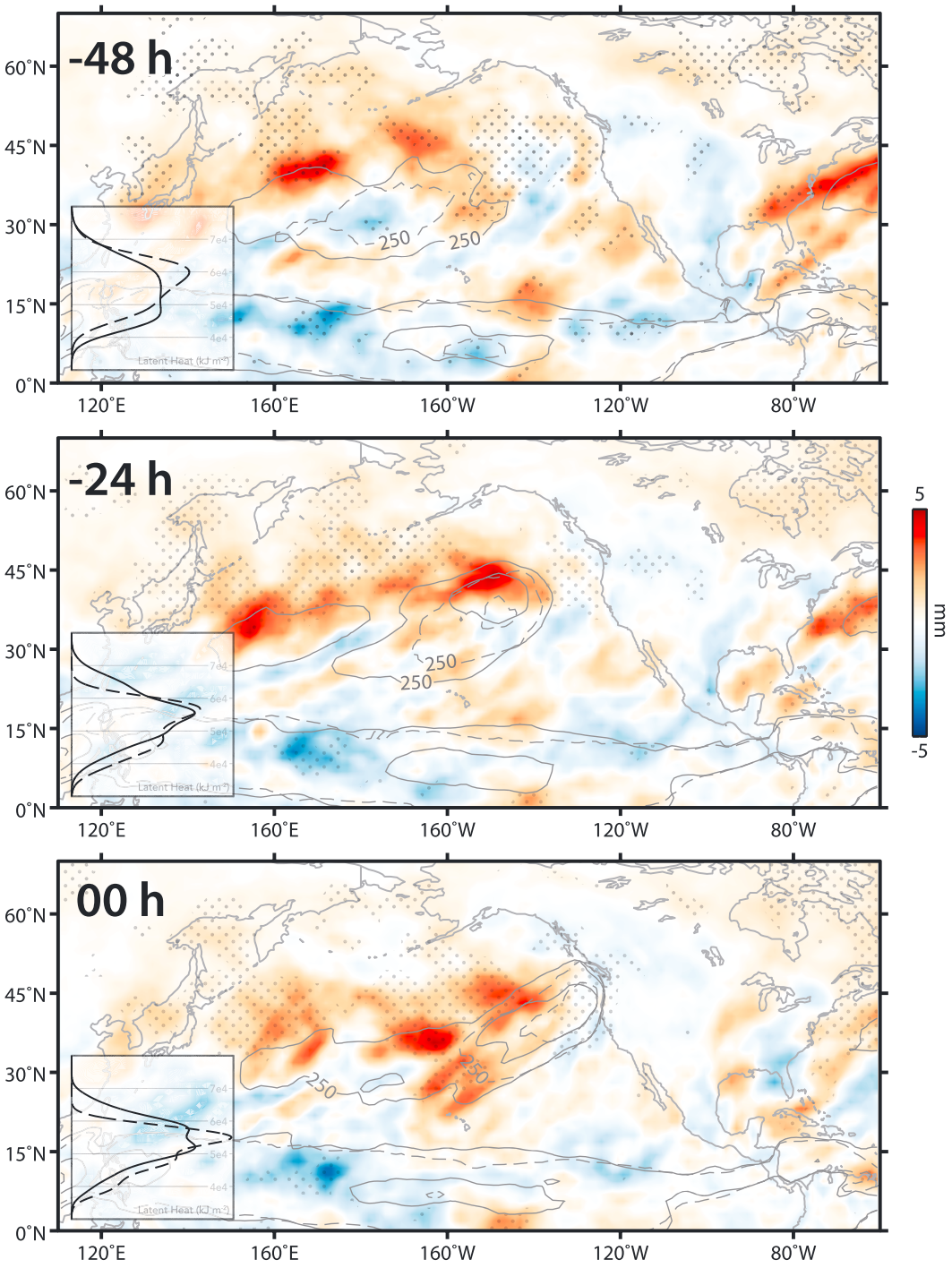

Figure 8. Same as Figure 3 but for the difference between persistent and nonpersistent analogues at −48, −24, and 00 h prior to landfall. Shading shows the difference in PW (mm) and contours show MF for persistent events (solid), and their nonpersistent analogues (dashed) (kg m^{-1} s^{-1}, intervals of 100 kg m^{-1} s^{-1}, starting from 250 kg m^{-1} s^{-1}). The inset in each panel shows the distribution of column-integrated latent heat within the composite persistent ARs (solid) and their nonpersistent analogues (dashed), calculated as the region colocated with MF ≥ 250 kg m^{-1} s^{-1} poleward of 20°N over the North Pacific basin.

the subsets overlap. Nonpersistent analogues, despite having similar dynamical patterns (as seen in 500 hPa geopotential height field) to persistent events, do not persist for longer than average along the coastline. Therefore, dry dynamics alone does not play a major role in the persistence of ARs.

Building on the results seen in Figure 3, we investigate the role of moisture in AR persistence. Figure 8 shows the difference in the development of persistent and nonpersistent analogues in PW (shading). For reference, dashed contouring shows MF for nonpersistent analogues and solid contouring shows MF for persistent events. The insets in each panel of Figure 8 show probability density functions of the column-integrated latent heat associated with the composite ARs in each panel. At all stages of development, persistent events are associated with higher moisture content over the extratropical North Pacific. Atmospheric moisture is elevated 48 h prior to landfall. As the composite AR moves eastward, the plume of MF marking the position of the AR is colocated with higher moisture content and the magnitude of the difference in moisture content between the two data sets increases.

4. Conclusions

Persistent landfalling AR events have a large hydrological impact on the western coastline of North America. Here we use a unique data set to investigate the duration of AR events and to quantify how persistent ARs are different from all ARs. The data set used in this research shows excellent agreement with existing records of landfalling events.

Our results highlight the large-scale differences of persistent AR events. Compared to all ARs, composite analysis show significant differences in thermodynamic and dynamic fields. PW and MF anomalies show a pattern characteristic of Pineapple Express events, with increased moisture and moisture flux extending from near Hawaii toward the Pacific Northwest. These anomalies are consistent with increased anticyclonic RWB, a perturbed upper level jet and a deeper low-pressure center to the north of the MF plume. Positive precipitation anomalies are centered along the Pacific Northwest and suggest a regional preference for persistent AR events. Comparison of the total number of persistent events to make landfall along the north coast to those impacting the south coast show a clear preference for the northern region. Analysis of anticyclonic RWB for persistent events shows both an eastward shift and an increase in frequency.

Investigation of the mechanisms contributing to AR persistence through analogue analysis shows that persistence is most likely related to the feedback of AR moisture supply on dynamics rather dry dynamics by itself. The magnitude of the difference in moisture between persistent and nonpersistent analogues is striking and it is apparent in the development of ARs over the basin. This analysis is limited by the consideration of only similarity of the nonpersistent analogues to persistent events.

Our results highlight the importance of moisture for the subset of persistent landfalling AR events. Recent work in *Payne and Magnusdottir* [2015], *Gao et al.* [2015], and *Warner et al.* [2015] have shown that at the end of the century ARs are projected to transport more moisture even though the frequency of ARs does not change considerably. It is possible that ARs may become more persistent in a warmer and moister climate, which has important implications for climate impacts.

Acknowledgments
We thank Marty Ralph and Scott Sellars, for a helpful discussion, and Julien Cattiaux, for his advice on using the analogue method. This research was supported by NSF grants AGS-1206120 and AGS-1407360 and NOAA Award NA15OAR4310164. All data used in this research are cited in *Rienecker et al.* [2011] and in *Guan and Waliser* [2015] and are referred to in the reference list. We also thank the three anonymous reviewers who contributed valuable suggestions.

References

Dettinger, M. D. (2011), Climate change, atmospheric rivers, and floods in California—A multimodel analysis of storm frequency and magnitude changes, *J. Am. Water Resour. Assoc.*, *47*(3), 514–523, doi:10.1111/j.1752-1688.2011.00546.x.

Dettinger, M. D., F. M. Ralph, T. Das, P. J. Neiman, and D. R. Cayan (2011), Atmospheric rivers, floods and the water resources of California, *Water*, *3*(2), 445–478, doi:10.3390/w3020445.

Dettinger, M. D. (2013), Atmospheric rivers as drought busters on the U.S. West Coast, *J. Hydrometeorol.*, *14*, 1721–1732, doi:10.1175/JHM-D-13-02.1.

Drouard, M., G. Riviere, and P. Arbogast (2013), The North Atlantic Oscillation response to large-scale atmospheric anomalies in the Northeastern Pacific, *J. Atmos. Sci.*, *70*, 2854–2874, doi:10.1175/JAS-D-12-0351.1.

Galewsky, J., and A. Sobel (2005), Moist dynamics and orographic precipitation in Northern and Central California during the New Years flood of 1997, *Mon. Weather Rev.*, *133*(6), 1594–1612, doi:10.1175/MWR2943.1.

Gao, Y., J. Lu, L. Ruby Leung, Q. Yang, S. Hagos, and Y. Qian (2015), Dynamical and thermodynamical modulations on future changes of landfalling atmospheric rivers over western North America, *Geophys. Res. Lett.*, *42*, 7179–7186, doi:10.1002/2015GL065435.

Guan, B., N. P. Molotch, D. E. Waliser, E. J. Fetzer, and P. J. Neiman (2010), Extreme snowfall events linked to atmospheric rivers and surface air temperature via satellite measurements, *Geophys. Res. Lett.*, *37*, L20401, doi:10.1029/2010GL044696.

Guan, B., and D. E. Waliser (2015), Detection of atmospheric rivers; evaluation and application of an algorithm for global studies, *J. Geophys. Res. Atmos.*, *120*, 514–535, doi:10.1002/2015JD024257.

Jackson, D. L., M. Hughes, and G. A. Wick (2016), Evaluation of landfalling atmospheric rivers along the U.S. West Coast in reanalysis data sets, *J. Geophys. Res. Atmos.*, *121*, 2705–2718, doi:10.1002/2015JD024412.

Lavers, D. A., G. Villarini, R. P. Allan, E. F. Wood, and A. J. Wade (2012), The detection of atmospheric rivers in atmospheric reanalyses and their links to British winter floods and the large-scale climatic circulation, *J. Geophys. Res.*, *117*, D20106, doi:10.1029/2012JD018027.

Lackmann, G. M., and J. R. Gyakum (1999), Heavy cold-season precipitation in the Northwestern United States: Synoptic climatology and an analysis of the flood of 17–18 January 1986, *Weather Forecasting*, *14*, 687–700, doi:10.1175/1520-0434(1999)014<0687:HCSPIT>2.0.CO;2.

Leung, L. R., and Y. Qian (2009), Atmospheric rivers induced heavy precipitation and flooding in the Western U.S. simulated by the WRF regional climate model, *Geophys. Res. Lett.*, *36*, L03820, doi:10.1029/2008GL036445.

Lorenz, E. N. (1969), Atmospheric predictability as revealed by naturally occurring analogues, *J. Atmos. Sci.*, *26*(636–646), doi:10.1175/1520-0469(1969)26<636:APARBN>2.0.CO;2.

McIntyre, M. E., and T. N. Palmer (1983), Breaking planetary waves in the stratosphere, *Nature*, *305*, 593–600, doi:10.1038/305593a0.

Moore, B. J., P. J. Neiman, F. M. Ralph, and F. E. Barthold (2012), Physical processes associated with heavy flooding rainfall in Nashville, Tennessee, and vicinity during 1–2 May 2010: The role of an atmospheric river and mesoscale convective systems, *Mon. Weather Rev.*, *140*(2), 358–378, doi:10.1175/MWR-D-11-00126.1.

Mundhenk, B. D., E. A. Barnes, and E. D. Maloney (2016), All-season climatology and variability of atmospheric river frequencies over the North Pacific, *J. Clim.*, *29*, 4885–4903, doi:10.1175/JCLI-D-15-0655.1.

Neiman, P. J., F. M. Ralph, G. A. Wick, Y.-H. Kuo, T.-K. Wee, Z. Ma, G. H. Taylor, and M. D. Dettinger (2008a), Diagnosis of an intense atmospheric river impacting the Pacific Northwest: Storm summary and offshore vertical structure observed with Cosmic satellite retrievals, *Mon. Weather Rev.*, *136*(11), 4398–4420, doi:10.1175/2008MWR2550.1.

Neiman, P. J., F. M. Ralph, G. A. Wick, J. D. Lundquist, and M. D. Dettinger (2008b), Meteorological characteristics and overland precipitation impacts of atmospheric rivers affecting the West Coast of North America based on eight years of SSM/I satellite observations, *J. Hydrometeorol.*, *9*(1), 22–47, doi:10.1175/2007JHM855.1.

Neiman, P. J., L. J. Schick, F. M. Ralph, M. Hughes, and G. A. Wick (2011), Flooding in Western Washington: The connection to atmospheric rivers, *J. Hydrometeorol.*, *12*(6), 1337–1358, doi:10.1175/2011JHM1358.1.

Payne, A. E., and G. Magnusdottir (2014), Dynamics of landfalling atmospheric rivers over the North Pacific in 30 years of MERRA reanalysis, *J. Clim.*, *27*(18), 7133–7150, doi:10.1175/JCLI-D-14-00034.1.

Payne, A. E., and G. Magnusdottir (2015), An evaluation of atmospheric rivers over the North Pacific in CMIP5 and their response to warming under RCP 8.5, *J. Geophys. Res. Atmos.*, *120*(21), 11,173–11,190, doi:10.1002/2015JD023586.

Ralph, F., P. J. Neiman, G. A. Wick, S. I. Gutman, M. D. Dettinger, D. R. Cayan, and A. B. White (2006), Flooding on California's Russian River: Role of atmospheric rivers, *Geophys. Res. Lett.*, *33*, L13801, doi:10.1029/2006GL026689.

Ralph, F. M., T. Coleman, P. J. Neiman, R. J. Zamora, and M. D. Dettinger (2013), Observed impacts of duration and seasonality of atmospheric-river landfalls on soil moisture and runoff in coastal Northern California, *J. Hydrometeorol.*, *14*(2), 443–459, doi:10.1175/JHM-D-12-076.1.

Ralph, F. M., and M. D. Dettinger (2012), Historical and national perspectives on extreme West Coast precipitation associated with atmospheric rivers during December 2010, *Bull. Am. Meteorol. Soc.*, *93*(6), 783–790, doi:10.1175/BAMS-D-11-00188.1.

Ralph, F. M., P. J. Neiman, G. N. Kiladis, K. Weickmann, and D. W. Reynolds (2011), A multiscale observational case study of a Pacific atmospheric river exhibiting tropicalextratropical connections and a mesoscale frontal wave, *Mon. Weather Rev.*, *139*(4), 1169–1189, doi:10.1175/2010MWR3596.1.

Ralph, F. M., P. J. Neiman, D. E. Kingsmill, P. O. G. Persson, A. B. White, E. T. Strem, E. D. Andrews, and R. C. Antweiler (2003), The impact of a prominent rain shadow on flooding in California's Santa Cruz Mountains: A CALJET case study and sensitivity to the ENSO cycle, *J. Hydrometeorol.*, *4*(6), 1243–1264, doi:10.1175/1525-7541(2003)004<1243:TIOAPR>2.0.CO;2.

Ralph, F. M., P. J. Neiman, and R. Rotunno (2005), Dropsonde observations in low-level jets over the northeastern Pacific Ocean from CALJET-1998 and PACJET-2001: Mean vertical-profile and atmospheric-river characteristics, *Mon. Weather Rev.*, *133*(4), 889–910, doi:10.1175/MWR2896.1.

Ralph, F. M., P. J. Neiman, and G. A. Wick (2004), Satellite and CALJET aircraft observations of atmospheric rivers over the eastern North Pacific ocean during the winter of 1997/98, *Mon. Weather Rev.*, *132*(7), 1721–1745, doi:10.1175/1520-0493(2004)132<1721:SACAOO>2.0.CO;2.

Ramos, A. M., R. M. Trigo, M. L. R. Liberato, and R. Tomé (2015), Daily precipitation extreme events in the Iberian Peninsula and its association with atmospheric rivers, *J. Hydrometeorol.*, *16*, 579–597, doi:10.1175/JHM-D-14-0103.1.

Rienecker, M. M., et al. (2011), MERRA: NASA's Modern-Era Retrospective Analysis for Research and Applications, *J. Clim.*, *24*(14), 3624–3648, doi:10.1175/JCLI-D-11-00015.1.

Rivera, E. R., F. Dominguez, and C. L. Castro (2014), Atmospheric rivers and cool season extreme precipitation events in the Verde River basin of Arizona, *J. Hydrometeorol.*, *15*(2), 813–829, doi:10.1175/JHM-D-12-0189.1.

Rutz, J. J., W. J. Steenburgh, and F. M. Ralph (2014), Climatological characteristics of atmospheric rivers and their inland penetration over the western United States, *Mon. Weather Rev.*, *142*(2), 905–921, doi:10.1175/MWR-D-13-00168.1.

Ryoo, J.-M., Y. Kaspi, D. W. Waugh, G. N. Kiladis, D. E. Waliser, E. J. Fetzer, and J. Kim (2013), Impact of Rossby wave breaking on U.S. West Coast winter precipitation during ENSO events, *J. Clim.*, *26*(17), 6360–6382, doi:10.1175/JCLI-D-12-00297.1.

Smith, B. L., S. E. Yuter, P. J. Neiman, and D. E. Kingsmill (2010), Water vapor fluxes and orographic precipitation over Northern California associated with a landfalling atmospheric river, *Mon. Weather Rev.*, *138*(1), 74–100, doi:10.1175/2009MWR2939.1.

Strong, C., and G. Magnusdottir (2008a), How Rossby wave breaking over the Pacific forces the North Atlantic Oscillation, *Geophys. Res. Lett.*, *35*(10), 1–5, doi:10.1029/2008GL033578.

Strong, C., and G. Magnusdottir (2008b), Tropospheric Rossby wave breaking and the NAO/NAM, *J. Atmos. Sci.*, *65*(9), 2861–2876, doi:10.1175/2008JAS2632.1.

Vautard, R., and P. Yiou (2009), Control of recent European surface climate change by atmospheric flow, *Geophys. Res. Lett.*, *36*, L22702, doi:10.1029/2009GL040480.

Warner, M. D., C. F. Mass, and E. P. Salathé (2012), Wintertime extreme precipitation events along the Pacific Northwest coast: Climatology and synoptic evolution, *Mon. Weather Rev.*, *140*(7), 2021–2043, doi:10.1175/MWR-D-11-00197.1.

Warner, M. D., C. F. Mass, and E. P. Salathé (2015), Changes in Winter Atmospheric Rivers along the North American West Coast in CMIP5 Climate Models, *J. Hydrometeorol.*, *16*(1), 118–128, doi:10.1175/JHM-D-14-0080.1.

Waugh, D. W., and L. M. Polvani (2000), Climatology of intrusions into the tropical upper troposphere, *Geophys. Res. Lett.*, *27*(23), 3857–3860, doi:10.1029/2000GL012250.